

# Commensurability in One Dimension and the Josephson Junction Ladder

Colin Denniston<sup>1,2,\*</sup> and Chao Tang<sup>2</sup>

<sup>1</sup>*Department of Physics, Princeton University, Princeton, New Jersey 08544*

<sup>2</sup>*NEC Research Institute, 4 Independence Way, Princeton, New Jersey 08540*

(May 15, 2018)

## Abstract

We study a Josephson junction ladder in a magnetic field in the absence of charging effects via a transfer matrix formalism. The eigenvalues of the transfer matrix are found numerically, giving a determination of the different phases of the ladder. The spatial periodicity of the ground state exhibits a devil's staircase as a function of the magnetic flux filling factor  $f$ . If the transverse Josephson coupling is varied a continuous superconducting-normal transition in the transverse direction is observed, analogous to the breakdown of the KAM trajectories in dynamical systems. We also examine how these properties may be affected by a current injected along the ladder.

74.50.+r, 05.20.-y, 64.70.Rh

## I. INTRODUCTION

Two-dimensional arrays of Josephson junctions have attracted much recent theoretical and experimental attention [1]. Interesting physics arises as a result of competing vortex-vortex and vortex-lattice interactions. It is also considered to be a convenient experimental realization of the frustrated XY models. In this paper, we expand and elaborate on our previous letter [2] on the simplest of such system, namely the Josephson junction ladder (JLL) [3–5] shown in Figure 1.

To construct the system, superconducting elements are placed at the ladder sites. Below the bulk superconducting-normal transition temperature, the state of each element is described by its charge and the phase of the superconducting wave function [6]. In this paper we neglect charging effects, which corresponds to the condition that  $4e^2/C \ll J$ , with  $C$  being the capacitance of the element and  $J$  the Josephson coupling. Let  $\theta_j$  ( $\theta'_j$ ) denote the phase on the upper (lower) branch of the ladder at the  $j$ 'th rung. The Hamiltonian for the array [7] can be written in terms the gauge invariant phase differences,  $\gamma_j = \theta_j - \theta_{j-1} - (2\pi/\phi_0) \int_{j-1}^j A_x dx$ ,  $\gamma'_j = \theta'_j - \theta'_{j-1} - (2\pi/\phi_0) \int_{j-1}^j A_x dx$ , and  $\alpha_j = \theta'_j - \theta_j - (2\pi/\phi_0) \int_j^{j'} A_y dx$ :

$$\mathcal{H} = - \sum_j (J_x \cos \gamma_j + J_x \cos \gamma'_j + J_y \cos \alpha_j), \quad (1)$$

where  $A_x$  and  $A_y$  are the components of the magnetic vector potential along and transverse to the ladder, respectively, and  $\phi_0$  the flux quantum. The sum of the phase differences around a plaquette is constrained by

$$\gamma_j - \gamma'_j + \alpha_j - \alpha_{j-1} = 2\pi(f - n_j), \quad (2)$$

where  $n_j = 0, \pm 1, \pm 2, \dots$  is the vortex occupancy number and  $f = \phi/\phi_0$  with  $\phi$  being the magnetic flux through a plaquette. With this constraint, it is convenient to write Eq. (1) in the form

$$\mathcal{H} = -J \sum_j \{ 2 \cos \eta_j \cos [(\alpha_{j-1} - \alpha_j)/2 + \pi(f - n_j)] + J_t \cos \alpha_j \}, \quad (3)$$

where  $\eta_j = (\gamma_j + \gamma'_j)/2$ ,  $J = J_x$  and  $J_t = J_y/J_x$ . The Hamiltonian is symmetric under  $f \rightarrow f + 1$  with  $n_j \rightarrow n_j + 1$ , and  $f \rightarrow -f$  with  $n_j \rightarrow -n_j$ , thus it is sufficient to study only the region  $0 \leq f \leq 0.5$ . Since in one dimension ordered phases occur only at zero temperature, the main interest is in the ground states of the ladder and the low temperature excitations. Note that in Eq. (3)  $\eta_j$  decouples from  $\alpha_j$  and  $n_j$ , so that all the ground states have  $\eta_j = 0$  to minimize  $\mathcal{H}$ . The ground states will be among the solutions to the current conservation equations  $\partial\mathcal{H}/\partial\alpha_j = 0$ :

$$J_t \sin \alpha_j = \sin[(\alpha_{j-1} - \alpha_j)/2 + \pi(f - n_j)] - \sin[(\alpha_j - \alpha_{j+1})/2 + \pi(f - n_{j+1})]. \quad (4)$$

For any given  $f$  there are a host of solutions to Eq. (4). The solution that minimizes the energy must be selected to obtain the ground state.

If one expands the  $\cos[(\alpha_{j-1} - \alpha_j)/2 + \pi(f - n_j)]$  term in Eq. (3) about its maximum and set  $\eta_j = 0$ , the discrete sine-Gordon model (DSG) is obtained:

$$\mathcal{H} = -J \sum_j \left\{ \frac{1}{2} [(\alpha_{j-1} - \alpha_j)/2 + \pi f]^2 + J_t \cos \alpha_j \right\}, \quad (5)$$

A vortex ( $n_j = 1$ ) in the JJJ corresponds to a kink in the DSG (in the DSG the  $\alpha$  absorb the  $n_j$  and are no longer restricted to  $(-\pi, \pi]$ ). Kardar [3] used this analogy to argue that this system should show similar behavior to the DSG which has been studied by several authors [8–10]. This analogy is only valid for  $J_t$  very small so that the inter-plaquette term dominates the behavior of the system making the expansion about its maximum a reasonable assumption. However, much of the interesting behavior of the DSG occurs in regions of large  $J_t$  ( $J_t \sim 1$ ). Furthermore, much of the work by Aubry [8] on the DSG relies on the convexity of the coupling potential which we do not have in the JJJ.

In this paper we formulate the problem in terms of a transfer matrix obtained from the full partition function of the ladder. The eigenvalues and eigenfunctions of the transfer matrix are found numerically to determine the phases of the ladder as functions of  $f$  and  $J_t$ . We find that the spatial periodicity of the ground states goes through a devil's staircase

as a function of  $f$ . We then study the properties of various ground states and the low temperature excitations. As  $J_t$  is varied, all incommensurate ground states are found to undergo a superconducting-normal transition at certain  $J_t$  which depends on  $f$ . In the last section we discuss the effects of a current.

## II. TRANSFER MATRIX FORMULATION

The partition function for the ladder, with periodic boundary conditions is

$$\mathcal{Z} = \prod_i^N \int_{-\pi}^{\pi} \sum_{\{n_i\}} d\alpha_i d\eta_i \exp \{K(2 \cos \eta_i \cos[(\alpha_{i-1} - \alpha_i)/2 + \pi(f - n_i)] + J_t \cos \alpha_i)\}. \quad (6)$$

where  $K = J/k_B T$ . The  $\eta_i$  can be integrated out and  $n_i$  summed over, resulting in a simple transfer matrix formalism for the partition function involving only the transverse phase differences:  $\mathcal{Z} = \prod_i^N \int_{-\pi}^{\pi} d\alpha_i P(\alpha_{i-1}, \alpha_i) = \text{Tr} \hat{P}^N$ . The transfer matrix elements  $P(\alpha, \alpha')$  are

$$P(\alpha, \alpha') = 4\pi \exp[K J_t (\cos \alpha + \cos \alpha')/2] I_0(2K \cos[(\alpha - \alpha')/2 + \pi f]), \quad (7)$$

where  $I_0$  is the zeroth order modified Bessel function ( $I_0(x) = \frac{1}{\pi} \int_0^\pi \exp(x \cos \eta) d\eta$ ). Note that the elements of  $\hat{P}$  are real and positive, so that its largest eigenvalue  $\lambda_0$  is real, positive and non-degenerate. However, since  $\hat{P}$  is not symmetric (except for  $f = 0$  and  $f = 1/2$ ) other eigenvalues can form complex conjugate pairs. As we will see from the correlation function, these complex eigenvalues determine the spatial periodicity of the ground states.

The two point correlation function of  $\alpha_j$ 's is

$$\begin{aligned} \langle e^{i(\alpha_0 - \alpha_l)} \rangle &= \lim_{N \rightarrow \infty} \frac{\left( \prod_i^N \int_{-\pi}^{\pi} d\alpha_i P(\alpha_{i-1}, \alpha_i) \right) e^{i(\alpha_0 - \alpha_l)}}{\mathcal{Z}} \\ &= \sum_n c_n \left( \frac{\lambda_n}{\lambda_0} \right)^l, \end{aligned} \quad (8)$$

where the  $\lambda_n$  are the eigenvalues ( $|\lambda_n| \geq |\lambda_{n+1}|$  and  $n = 0, 1, 2, \dots$ ), and the constants  $c_n = \int_{-\pi}^{\pi} d\alpha' \psi_0^L(\alpha') e^{i\alpha'} \psi_n^R(\alpha') \int_{-\pi}^{\pi} d\alpha \psi_n^L(\alpha) e^{-i\alpha} \psi_0^R(\alpha)$ . (Note that since  $\hat{P}$  is not symmetric both right  $\psi_n^R$  and left  $\psi_n^L$  eigenfunctions are needed.) If  $\lambda_1$  is real and  $|\lambda_1| > |\lambda_2|$ , Eq. (8) simplifies for large  $l$  to

$$\langle e^{i(\alpha_0 - \alpha_l)} \rangle = c_0 + c_1 \left( \frac{\lambda_1}{\lambda_0} \right)^l, \quad |\lambda_1| > |\lambda_2|.$$

If  $\lambda_1 = \lambda_2^* = |\lambda_1|e^{i2\pi\Xi}$ , Eq. (8) for large  $l$  is

$$\langle e^{i(\alpha_0 - \alpha_l)} \rangle = c_0 + \left( c_1 e^{i2\pi\Xi l} + c_2 e^{-i2\pi\Xi l} \right) \left| \frac{\lambda_1}{\lambda_0} \right|^l, \quad \lambda_1 = \lambda_2^*.$$

Note that while the correlation length is given by  $\xi = [\ln |\lambda_0/\lambda_1|]^{-1}$  the quantity  $\Xi = \text{Arg}(\lambda_1)/2\pi$  determines the spatial periodicity of the state. For example, Figure 2 shows the full correlation function (not just the first two terms) for a three periodic state,  $\Xi = 1/3$ . We see that the correlation function has three branches corresponding to  $\langle e^{i(\alpha_0 - \alpha_{3n})} \rangle$ ,  $\langle e^{i(\alpha_0 - \alpha_{3n+1})} \rangle$ , and  $\langle e^{i(\alpha_0 - \alpha_{3n+2})} \rangle$  with  $n = 0, 1, 2, \dots$ .

It is fairly easy to find the eigenvalues and eigenvectors of the transfer matrix numerically to very high accuracy (see the Appendix). For  $f$  smaller than a critical value  $f_{c1}$  which depends on  $J_t$ , we find that both  $\lambda_1$  and  $\lambda_2$  are real. These two eigenvalues become degenerate at  $f_{c1}$ , and then bifurcate into a complex conjugate pair.  $\Xi$  as a function of  $f$  is shown in Figure 3 for several different values of  $J_t$ . The shape of these curves is generally referred to as a devil's staircase. The steps of the staircase are at  $\Xi = p/q$ , where  $p$  and  $q$  are integers. These are commensurate states with  $p$  vortices in each unit cell which consists of  $q$  plaquettes. For small  $J_t$ , the flat steps are connected by fairly smooth curves; most states on the  $\Xi - f$  curve are incommensurate states. As  $J_t$  increases, more and more steps appear and grow at the expense of the smooth regions. It appears that at  $J_t = J_t^c \approx 0.5$  the staircase becomes complete, i.e. there is a step for every rational  $\Xi$  and the set of  $f$  which correspond to irrational  $\Xi$  has zero measure. For  $J_t > J_t^c$ , the staircase becomes over-complete, i.e. steps of lower order rationals grow and steps of higher order rationals disappear [11]. A phase diagram can be constructed with the phase boundaries at the step edges, as shown in Figure 4.

Another important characterization of a state is the phase density  $\rho(\alpha)$ :  $\rho(\alpha)d\alpha$  is the average fraction of all sites in the ladder with  $\alpha < \alpha_i < \alpha + d\alpha$ . If  $\rho(\alpha)$  is a smooth function for  $\alpha \in (-\pi, \pi]$  at  $T = 0$ , the ground state energy is invariant under an adiabatic change of  $\alpha$ 's. Consequently, there is no phase coherence between upper and lower branches of the ladder and hence no superconductivity in the transverse direction. In this case, we say that

the  $\alpha$ 's are unpinned. If there exist finite intervals of  $\alpha$  on which  $\rho(\alpha) = 0$ , the  $\alpha$ 's are pinned and there will be phase coherence between the upper and lower branches. In terms of the transfer matrix, the phase density is the product of the left and right eigenfunctions of  $\lambda_0$  [12],  $\rho(\alpha) = \psi_0^L(\alpha)\psi_0^R(\alpha)$ .

### III. COMMENSURATE STATES

We first discuss the case where  $f < f_{c1}$ . These are the ‘‘Meissner’’ states in the sense that there are no vortices ( $n_i = 0$ ) in the ladder. The ground state is simply  $\alpha_i = 0$ ,  $\gamma_j = \pi f$  and  $\gamma'_j = -\pi f$ , so that there is a global ‘‘screening’’ current  $\pm J_x \sin \pi f$  in the upper and lower branches of the ladder [3]. The phase density  $\rho(\alpha) = \delta(\alpha)$ . The properties of the Meissner state can be studied by expanding Eq. (3) around  $\alpha_i = 0$ :

$$\mathcal{H}_M = (J/4) \sum_j [\cos(\pi f)(\alpha_{j-1} - \alpha_j)^2 + 2J_t \alpha_i^2]. \quad (9)$$

At finite temperature,  $\rho(\alpha) = \delta(\alpha)$  peaks become thermally broadened. The fluctuations about  $\alpha_i = 0$  in the  $J_t \alpha_i^2$  part of the energy of a single plaquette will be of order  $k_b T$  (from equipartition). Hence  $\delta \alpha_i \sim \sqrt{k_b T}$  is an estimate of the  $\rho(\alpha)$  peak width. The current conservation Eq. (4) becomes

$$\alpha_{j+1} = 2(1 + J_t / \cos \pi f) \alpha_j - \alpha_{j-1}. \quad (10)$$

Besides the ground state  $\alpha_j = 0$ , there are other two linearly independent solutions  $\alpha_j = e^{\pm j/\xi_M}$  of Eq. (10) which describe collective fluctuations about the ground state, where

$$\frac{1}{\xi_M} = \ln \left[ 1 + \frac{J_t}{\cos \pi f} + \sqrt{\frac{2J_t}{\cos \pi f} + \left( \frac{J_t}{\cos \pi f} \right)^2} \right]. \quad (11)$$

$\xi_M$  is the low temperature correlation length for the Meissner state. (Note that  $\xi_M < 1$  for  $J_t \sim 1$  making a continuum approximation invalid.) A comparison of  $\xi_M$  to the correlation length obtained from the transfer matrix (or from an exact solution of the Gaussian model (9) partition function [13]) shows that the two are indistinguishable for  $k_b T/J \leq 0.005$ . Note

that for finite  $J_t$  this model has no zero temperature phase transition in the sense that the correlation length remains finite as  $T \rightarrow 0$ . Furthermore, the correlation length diverges like  $1/\sqrt{2J_t}$  as  $J_t \rightarrow 0$ . (or more accurately, approaches the rigid rotator value of  $1/k_bT$ , as we shall see below.)

As  $f$  increases, the Meissner state becomes unstable to the formation of vortices. A vortex is constructed by patching the two vortex free solutions of the Eq. (10) together anti-symmetrically about the plaquette with the vortex. Using Eq. (4) for the matching condition,

$$-\sin(\alpha_* + \pi f) - \sin((e^{1/\xi_M} - 1)\alpha_*/2 + \pi f) + \sin \alpha_* = 0.$$

where  $\pm\alpha_*$  is the the value of  $\alpha_j$  on the plaquette enclosing the vortex. Expanded to second order, this gives

$$-4 \sin(\pi f) + [2 - (e^{1/\xi_M} + 1) \cos(\pi f)]\alpha_* + [1 + (e^{1/\xi_M} - 1)^2] \sin(\pi f)\alpha_*^2 = 0$$

To first order, the energy  $\epsilon_v$  of a single vortex is found to be

$$\epsilon_v = 4 \cos(\pi f) - 3\alpha_* \sin(\pi f)$$

The zero of  $\epsilon_v$  determines  $f_{c1}$ . This gives  $f_{c1} \approx 0.26$  for  $J_t = 1$ . Extending the calculation of  $\epsilon_v$  to second order gives  $f_{c1} \approx 0.28$  for  $J_t = 1$  which is in good agreement with the numerical result from the transfer matrix.

For  $f > f_{c1}$ ,  $\epsilon_v$  is negative and vortices are spontaneously created. When vortices are far apart their interaction is caused only by the exponentially small overlap. The corresponding repulsion energy is of the order  $J \exp(-l/\xi_M)$ , where  $l$  is the distance between vortices. At finite temperatures and low densities, the vortices will be able to overcome a weak pinning potential and will move around fairly freely in the  $l$  sites separating the vortices. This leads to a free energy per plaquette [10] of

$$F = \epsilon_v/l + Jc \exp(-l/\xi_M)/l - k_B T \ln l/l,$$

where  $c$  is a constant of order unity. Minimizing this free energy as a function of  $l$  and putting in the dependence of  $\epsilon_v$  near  $f_{c1}$  gives  $\langle n_j \rangle = l^{-1} = [\xi_M \ln |f_{c1} - f|]^{-1}$ , for  $(f - f_{c1})/k_B T \gg 1$ .

We now discuss the commensurate vortex states, taking the one with  $\Xi = 1/2$  as an example. This state has many similarities to the Meissner state but some important differences. The ground state is

$$(\alpha_0, n_0) = (\arctan [(2/J_t) \sin(\pi f)], 0), (\alpha_1, n_1) = (-\alpha_0, 1); (\alpha_{i\pm 2}, n_{i\pm 2}) = (\alpha_i, n_i);$$

so that there is a global screening current in the upper and lower branches of the ladder of  $\pm 2\pi J(f - 1/2)/\sqrt{4 + J_t^2}$  and the energy is  $\sqrt{1 + (2/J_t)^2 \sin^2(\pi f)}$ . Global screening, which is absent in an infinite 2D array, is the key reason for the existence of the steps at  $\Xi = p/q$ . It is easy to see that the symmetry of this  $\Xi = 1/2$  vortex state is that of the (antiferromagnetic) Ising model. The low temperature excitations are domain boundaries between the two degenerate ground states. The energy of the domain boundary  $J\epsilon_b$  can be estimated using similar methods to those used to derive  $\epsilon_v$  for the Meissner state. We found that  $\epsilon_b = \epsilon_b^0 - (\pi^2/\sqrt{4 + J_t^2})|f - 1/2|$ , where  $\epsilon_b^0$  depends only on  $J_t$ . Thus the correlation length diverges with temperature as  $\xi \sim \exp(2J\epsilon_b/k_B T)$ . The transition from the  $\Xi = 1/2$  state to nearby vortex states happens when  $f$  is such that  $\epsilon_b = 0$ ; it is similar to the transition from the Meissner state to its nearby vortex states. All other steps  $\Xi = p/q$  can be analyzed similarly. For comparison, we have evaluated  $\xi$  for various values of  $f$  and  $T$  from the transfer matrix and found that  $\xi$  fits  $\xi \sim \exp(2J\epsilon_b/k_B T)$  (typically over several decades) at low temperature. The value of  $\epsilon_b$  as a function of  $f$  is shown in Fig. 5 for  $J_t = 1$ . The agreement with the above estimate for the  $\Xi = 1/2$  step is excellent.

Another feature that can be fairly easily understood is the relative heights of the tips of the peaks in Fig. 5 for states with  $\Xi = 1/q$ . These states consist of one vortex every  $q$  plaquettes in the ground state configuration. The lowest energy domain wall consists of having one spacing that is  $q - 1$  rather than  $q$  between two consecutive vortices. This should cost an interaction energy of about  $\tau \sim \exp(-q/l_0)$  with  $l_0 \approx \xi_M$  of Eq. (11) and indeed the tips of the peaks in Fig. 5 for states with  $\Xi = 1/q$  fit this relationship quite well.

The low temperature transverse resistance should be proportional to the thermal activation rate of domain walls:  $R_t \sim \exp(-2J\epsilon_b/k_B T)$  (with  $\epsilon_b$  replaced with  $\epsilon_v$  for the Meissner



state). This facilitates direct comparison with experiment [5].

#### IV. INCOMMENSURATE STATES AND PINNING-DEPINNING TRANSITION

We now discuss the incommensurate states and superconducting-normal transitions in the transverse direction in these states. An incommensurate state is a state for which  $\Xi$  is an irrational number. For  $J_t = 0$ , the ground state has  $\gamma_i = \gamma'_i = 0$  and the  $\alpha_i$  are just pseudo- or slave variables determined by the constraint Eq.(2):

$$\alpha_j = 2\pi f j + \alpha_0 - 2\pi \sum_{i=0}^{i=j} n_i. \quad (12)$$

The average vortex density  $\langle n_j \rangle$  is  $f$ ; screening currents are absent.  $\alpha_0$  in Eq. (12) is arbitrary; the  $\alpha$ 's are "unpinned" for all  $f$ . The system is simply two uncoupled 1D XY chains (or rigid rotor model), so that the correlation length  $\xi = 1/k_B T$  (see for instance Ref. [14]). The system is superconducting at zero temperature along the ladder, but not in the transverse direction. As  $J_t$  rises above zero we observe a distinct difference between the system at rational and irrational values of  $f$ . For  $f$  rational, the  $\alpha$ 's become pinned for  $J_t > 0$  ( $\rho(\alpha)$  is a finite sum of delta functions) and the ladder is superconducting in *both* the longitudinal and transverse directions at zero temperature. For the  $f = 0$  case, the correlation length drops from the rigid rotor value of  $\xi = 1/k_b T$  to the value found above in Eq.(11) like  $T^{-1/2}$ .

The behavior for irrational  $f$  is illustrated in the following for the state with  $\Xi = a_g$ , where  $a_g = (3 - \sqrt{5})/2$  (one minus the Golden Mean). Fig. 6 displays  $\rho(\alpha)$  for several different  $J_t$  at  $\Xi = a_g$ . We see that the zero-frequency phonon mode (the smoothness of  $\rho(\alpha)$ ) persists for small  $J_t > 0$  until a critical value  $J_t^c(f) \approx 0.5$  where the  $\alpha$ 's become pinned and the ladder becomes superconducting in the transverse direction. In the DSG, the pinning transition of this state coincides with the devil's staircase of Fig. 3 becoming complete [8,9] (If the  $\alpha_j$ 's are pinned in this state, then all incommensurate states should be pinned). From Fig. 6 we see that this transition is a transition where the integration

measure  $\rho(\alpha)$  in the partition function goes from a set of measure one on  $[-\pi, \pi)$  to a set of measure zero (at  $T \rightarrow 0$ ). As one approaches the transition from  $J_t < J_t^c$ ,  $\rho(\alpha) \rightarrow 0$  continuously almost everywhere in  $[-\pi, \pi)$ . As an order parameter for the transition, we use  $\rho(-\pi)$ . This is shown in Figure 7 at a number of temperatures approaching  $T = 0$ . At the same  $J_t$  the correlation length drops from the rigid rotor value of  $\xi = 1/(k_B T)$  continuously towards a value of a few tens of lattice constants. This is shown in Figure 8. For  $J_t < J_t^c$   $\xi = 1/(k_B T)$  is limited only by the temperature of the system. This is also true of the higher order correlation lengths,  $[\ln |\lambda_0/\lambda_n|]^{-1}$ ,  $n > 1$  in the unpinned phase which also diverge like  $1/(k_B T)$ .

Following standard scaling arguments one would expect  $\rho(-\pi)$  to scale according to

$$\rho(-\pi)(j, \xi) = j^\beta \tilde{f}(j\xi^{1/\nu}),$$

where  $j = J_t^c - J_t$  and  $\xi \sim j^{-\nu}$  for  $T = 0$  while  $\xi$  is a function of  $j$  and  $T$  for  $T > 0$ . For  $T \rightarrow 0$ ,  $\xi \rightarrow \infty$  in the unpinned phase and  $\rho(-\pi)$  should be independent of  $\xi$  implying  $\tilde{f}(y) \rightarrow \text{constant}$  as  $y \rightarrow \infty$  so that  $\rho(-\pi) \sim j^\beta$ . In the opposite extreme, with  $T$  fixed and  $j \rightarrow 0$ ,  $\rho(-\pi)$  is dominated by the finite  $\xi$  so that  $\tilde{f}(x) \rightarrow 1/x^\beta$  as  $x \rightarrow 0$  and  $\rho(-\pi) \sim \xi^{-\beta/\nu}$ . This allows us to define a more convenient scaling function  $f(x) = 1/x^\beta \tilde{f}(x)$  so that

$$\rho(-\pi)(j, \xi) = \xi^{-\beta/\nu} f(j\xi^{1/\nu}).$$

The results of this scaling, shown in the inset of Figure 7, gives  $\beta/\nu = 0.0926 \pm 0.0009$  and  $1/\nu = 0.352 \pm 0.001$ , or  $\beta = 0.263 \pm 0.003$  and  $\nu = 2.841 \pm 0.008$ .

A similar scaling can be applied to  $\xi$ :

$$\xi(j, T) = T^{-1}(a + b/\ln T)g(j\xi^{1/\nu})$$

where we have included the correction to scaling term  $b/\ln T$  which causes a slight improvement to the fit away from  $J_t^c$ . (A power law correction was also considered, but did not have a statistically significant coefficient.) The resulting scaling collapse is shown in the inset of Fig. 8. This does not really give us any new information, but does act as a check on the information from the scaling of  $\rho(-\pi)$ .

The pinning transition of the incommensurate states can be also studied using Eq. (4) which are equivalent to the two-dimensional map:

$$\sin \gamma_{j+1} = \sin \gamma_j - J_t \sin \alpha_j, \quad (13a)$$

$$\alpha_{j+1} = \alpha_j - 2\gamma_{j+1} + 2\pi(f - n_{j+1}). \quad (13b)$$

Vortices are required in order to keep  $\alpha_j$  in  $(-\pi, \pi]$ . Every trajectory of this map is a zero-temperature metastable state of the ladder. At  $J_t = 0$  the orbits of (13) for the incommensurate states will fill in a straight line  $\gamma = 0$  in the  $\gamma\alpha$  plane. As  $J_t$  increases, these Kolmogorov-Arnold-Moser (KAM) orbits become deformed but remain smooth with the energy remaining independent of  $\alpha_0$ . Once  $J_t$  exceeds a critical value the KAM curve breaks down into a Cantor set of measure zero, as shown in Figure 9. The disappearance of the zero-frequency phonon mode for irrational  $\Xi$ 's at finite small  $J_t^c(f)$  is equivalent to the breakdown of the Kolmogorov-Arnold-Moser (KAM) trajectories of the map [15].

However, we have been unable to find any connection between the exponents we found (describing the approach at  $\Xi = a_g$  to  $J_t^c$  and  $T = 0$ ) to those found in [15] for the approach to  $\Xi = a_g$  at  $J_t^c$  and  $T = 0$  for the standard map. If one expands the  $\sin \gamma_j \approx \gamma_j$  in (13) and redefine  $\gamma_j \rightarrow \gamma_j - \pi f$  one obtains the standard map, studied by several authors including [15,9]. If one compares the critical  $J_t^c$  to the equivalent value for the standard map ( $J_t = k_c/2$  in the language of [15]) one finds that they are identical. This is somewhat surprising. One might expect the two problems to be in the same universality class with related exponents but the location of the critical point normally depends on the details of the problem.

## V. EFFECT OF A CURRENT

We now turn to the subject of critical currents along the ladder. One can obtain an estimate for the critical current by performing a perturbation expansion (i.e.  $\{n_j\}$  remain fixed) around the ground state and imposing the current constraint of

$$\sin \gamma_j + \sin \gamma'_j = I. \quad (14)$$

Letting  $\delta\gamma_j$  and  $\delta\alpha_j$  be the change of  $\gamma_j$  and  $\alpha_j$  in the current carrying state, an expansion to first order gives

$$\begin{aligned} & \cos \gamma_{j-1} \delta\alpha_{j-1} + \cos \gamma_j \delta\alpha_{j+1} \\ & - (\cos \gamma_j + \cos \gamma_{j-1} + 2 \cos \alpha_j) \delta\alpha_j = 0, \end{aligned} \quad (15a)$$

$$\delta\gamma_j = \frac{1}{2}(\delta\alpha_{j+1} - \delta\alpha_j + \frac{I}{\cos \gamma_j}). \quad (15b)$$

Eq. (15a) is in the form of  $G \cdot \vec{\delta\alpha} = 0$ . If  $\det G \neq 0$ , then  $\delta\alpha_j = 0$  and  $\delta\gamma_j = I/2 \cos \gamma_j$ . The critical current can be estimated by the requirement that the  $\gamma_j$  do not pass through  $\pi/2$ , which gives  $I_c = 2(\pi/2 - \gamma_{\max}) \cos \gamma_{\max}$ , where  $\gamma_{\max} = \max_j(\gamma_j)$ . In all ground states we examined for  $J_t = 1.0$ , commensurate and incommensurate, we found that  $\gamma_{\max} < \pi/2$ , implying a finite critical current for all  $f$ .

The presence of a current can also have an effect analogous to weakening the transverse coupling  $J_t$ . One can get an approximate phase diagram in the  $I$ - $f$  plane, valid for very low temperature and  $I < I_c$ . To do this, rather than integrate out the  $\eta_i$  in Eq.(6), one can substitute the current constraint Eq.(14) and get the ‘‘partition’’ function for the current carrying states as

$$\mathcal{Z} = \prod_i^N \int_{-\pi}^{\pi} d\alpha_i 2 \exp(\beta J_t \cos \alpha_i) \cosh \left[ 2K \sqrt{\cos^2[(\alpha_{i-1} - \alpha_i)/2 + \pi f] - (I/J)^2/4} \right]. \quad (16)$$

Again, this is in the form of a product of transfer matrices and can be easily solved by the same techniques as before (see the appendix). The resulting phase diagram is shown in Figure 10 (compare to Fig. 4).

Comparing this diagram to Fig. 4 one can see that the increasing  $I$  in Fig. 10 has the same effect as decreasing  $J_t$  in Fig. 4. This opens the possibility of experimentally studying things like the pinning-depinning transition experimentally. In this case, the pinning-depinning transition would be driven by the longitudinal current, and a measurement in the transverse direction would be used to probe the coherence of the two chains.

This phase diagram in Fig. 10 should be taken too literally however as once the critical current for the system is exceeded, the current constraint of Eq.(14) is no longer valid and

the system can switch between metastable states or may change continuously between a very large number of states.

## VI. CONCLUSION AND ACKNOWLEDGMENTS

In conclusion, we have studied the equilibrium behavior of a Josephson junction ladder in a magnetic field in the absence of charging effects. Screening currents play an important role in this system, resulting in the spatial periodicity of the ground state climbing a devil's staircase as a function of  $f$ . Incommensurate states undergo a superconducting-normal transition in the transverse direction as  $J_t$  is increased, so that for  $J_t > J_t^c \approx 0.5$  the ladder is superconducting in both the longitudinal and transverse directions for all  $f$ . The critical current along the ladder is found to be finite for all  $f$ . Finally, although in one dimension there is no phase transition and long range order at finite temperature, our study showed that the correlation lengths in vortex states are extremely long for reasonably low temperatures. Thus one could test experimentally the predictions for the vortex configuration by, for instance, direct imaging via a scanning Hall-probe microscope or measuring the fractional giant Shapiro steps [16].

We thank Sue Coppersmith, Xinsheng Ling, and Qian Niu for valuable discussions.

## APPENDIX A: NUMERICAL SOLUTION TO INTEGRAL EIGENVALUE EQUATIONS

To find the eigenvalues of the transfer matrix (7), we used the Nystrom method with  $n$ -point Gauss-Legendre quadrature [17]. The resulting matrix eigenvalue problem was then solved using the routines in LAPACK. It is worth describing this method here as it is fairly simple. We should also note that this method is quite fast, compared to methods such as the effective potential methods used by Mazo et al. in Ref. [4]. Indeed one can generate phase diagrams such as those in Fig. 3 in a few minutes or in Fig. 10 in a hour or so of computer time (on an SGI workstation).

The transfer matrix  $\hat{P}$  is not symmetric (except when  $f = 0$  or  $1/2$ ), and we will therefore require both right  $\psi_n$  and left  $\tilde{\psi}_n$  eigenvectors for the calculation of correlation functions. The eigenvalues and left and right eigenvectors are defined by the relations

$$\begin{aligned} \int_{-\pi}^{\pi} d\alpha' P(\alpha, \alpha') \psi_n(\alpha') &= \lambda_n \psi_n(\alpha) & (|\lambda_n| \geq |\lambda_{n+1}|) \\ \int_{-\pi}^{\pi} d\alpha \tilde{\psi}_n(\alpha) P(\alpha, \alpha') &= \lambda_n \tilde{\psi}_n(\alpha'). \end{aligned} \quad (\text{A1})$$

The left and right eigenvectors are orthonormal ( $\int d\alpha \tilde{\psi}_n(\alpha) \psi_{n'}(\alpha) = \delta_{nn'}$ ) and complete (In all cases examined, the eigenvalues, though possibly equal in magnitude as in a complex conjugate pair, were nondegenerate). Note that the elements of the transfer matrix  $\hat{P}$  are real and positive, so that the largest eigenvalue is real, positive and nondegenerate. Also, any complex eigenvalues will occur in complex conjugate pairs so that the partition function remains real and positive for any  $N$ .

The Nystrom method requires the choice of some approximate quadrature rule:

$$\lambda_n \psi_n(\alpha) = \int_{-\pi}^{\pi} d\alpha' P(\alpha, \alpha') \psi_n(\alpha') \approx \sum_{j=1}^n w_j P(\alpha, \alpha'_j) \psi_n(\alpha'_j) \quad (\text{A2})$$

Here the set  $\{w_j\}$  are the weights of the quadrature rule, while the  $n$  points  $\{\alpha'_j\}$  are the abscissas. Since the solution method involves  $O(n^3)$  operations it is worthwhile to use a high-order quadrature rule. For smooth, nonsingular problems Gaussian quadrature tends to be the best. Elements of the transfer matrix become increasingly singular as  $T \rightarrow 0$ , which produces computational difficulties. (For instance, a free energy per plaquette of 2.836 at  $k_b T/J = 0.004$  corresponds to  $\lambda_0 \sim 10^{308}$ , or close to overflow on the Silicon Graphics Indigo workstation used). Despite this problem, we found  $n$ -point Gauss-Legendre quadrature ( $n$  was typically 150 to 500) to give quite reasonable results. The largest errors tend to occur in the location of the edge of the steps of the devil's staircase, and even these errors are far too small to be visible on the plots. The lowest temperature achieved was  $k_b T/J = 0.0007$ , which we believe is sufficient to characterize the states of the zero temperature system (to achieve this temperature, a constant was added to the energy so that the ground state energy was near zero, thus helping to correct for the overflow problem).

Equation (A2) is a standard eigenvalue equation

$$\hat{\mathbf{P}} \cdot \psi = \lambda \psi \tag{A3}$$

which was solved using the routines in LAPACK (LAPACK library routines are provided on most workstation based systems and source code can be obtained free from netlib [18]). When making use of the eigenvectors (such as in the calculation of correlation functions) at points not included in the quadrature points one should make use of Eq.(A2) in order to maintain the full accuracy of the solution. In addition, in order to keep track of the weights, it is useful to symmetrize the weighting: defining the diagonal matrix  $\mathbf{D}^{1/2} = \text{diag}(\sqrt{w_j})$ . then the eigenvalue equation becomes

$$(\mathbf{D}^{1/2} \hat{\mathbf{P}} \mathbf{D}^{1/2}) \cdot (\mathbf{D}^{1/2} \psi) = \lambda (\mathbf{D}^{1/2} \psi),$$

which is in the form of a symmetric eigenvalue problem for  $f = 0, 1/2$ .

## REFERENCES

- \* Present Address: Dept. of Physics, Theoretical Physics, University of Oxford, 1 Keble Road, Oxford OX1 3NP.
- [1] For a general review, see *Physica B* **152**, 1-302 (1988).
- [2] C. Denniston and C. Tang, *Phys. Rev. Lett.* **75**, 3930 (1995).
- [3] M. Kardar, *Phys. Rev. B* **30**, 6368 (1984); *Phys. Rev. B* **33**, 3125 (1986).
- [4] E. Granato, *Phys. Rev. B* **42**, 4797 (1990); S. Ryu, W. Yu, and D. Stroud, *Phys. Rev. E* **53**, 2190, (1996); J. Mazo, F. Falo and L. Floria, *Phys. Rev. B* **52**, 10 433 (1995); J. Mazo and J. Ciria, *Phys. Rev. B* **54**, 16068 (1996).
- [5] H. Eikmans *et al.*, *Physica B* **165&166**, 1569 (1990); H. Eikmans and J. van Himbergen, *Phys. Rev. B* **41**, 8927 (1990).
- [6] P. W. Anderson, in *Lectures on the Many Body Problem*, edited by E.R. Caianiello (Academic Press, New York, 1964), Vol. 2, pp. 113.
- [7] M. Tinkham, *Introduction to Superconductivity*, (McGraw-Hill, New York, 1975).
- [8] S. Aubry and G. André, in *Group Theoretical Methods in Physics*, edited by Horowitz and Ne'eman, *Ann. Israel Phys. Soc.* **3**, 133 (1980); S. Aubry, *Ferroelectrics* **24**, 53 (1980); in *The Riemann Problem, Complete Integrability and Arithmetic Applications*, Vol. 925 of *Lecture Notes in Mathematics* (Springer-Verlag, 1982), pp. 221-245.
- [9] S.N. Coppersmith and D.S. Fisher, *Phys. Rev. B* **28**, 2566 (1983).
- [10] V.L. Pokrovsky, A.L. Talapov and P. Bak, in *Solitons*, edited by Trullinger *et al.*, (Elsevier, 1986), pp. 71-127.
- [11] We are grateful to S. Coppersmith for pointing out to us that in the limit of  $J_t \rightarrow \infty$ , only integer steps survive, so that  $\Xi = 0$  for  $f < 1/2$  and  $\Xi = 1$  for  $1/2 < f < 1$ .



- [12] R.A. Guyer and M.D. Miller, Phys. Rev. Lett. **42**, 718 (1979).
- [13] see for instance, G. Parisi, *Statistical Field Theory*, (Addison-Wesley,1988), pp. 227.
- [14] see for instance, Itzykson and Drouffe, *Statistical Field Theory* (Cambridge Univ. Press, 1989), pp. 40.
- [15] For scaling analysis of the breakdown of KAM trajectories in the “standard map”, see L.P. Kadanoff, Phys. Rev. Lett. **47**, 1641 (1981) and S.J. Shenker and L.P. Kadanoff, J. Stat. Phys. **27**, 631 (1982).
- [16] S.P. Benz *et al.*, Phys. Rev. Lett. **64**, 693 (1990); W. Yu *et al.*, Phys. Rev. B **45**, 12624 (1992).
- [17] L.M. Delves and J.L. Mohamed, *Computational Methods for Integral Equations* (Cambridge Univ. Press, 1985); or W.H. Press *et. al.*, *Numerical Recipes, 2nd Edition* (Cambridge Univ. Press, 1992).
- [18] see [http://csep1.phy.ornl.gov/cornell\\_proceedings/tutorials/Xnetlib/xnetlib\\_ov.html](http://csep1.phy.ornl.gov/cornell_proceedings/tutorials/Xnetlib/xnetlib_ov.html) .

FIGURES

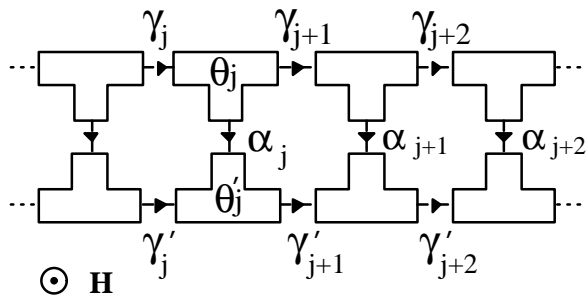


FIG. 1. The Josephson junction ladder is formed by the arrangement of the superconducting islands. The field  $\mathbf{H}$  is out of the page and the arrows indicate the direction of the gauge invariant phase differences.

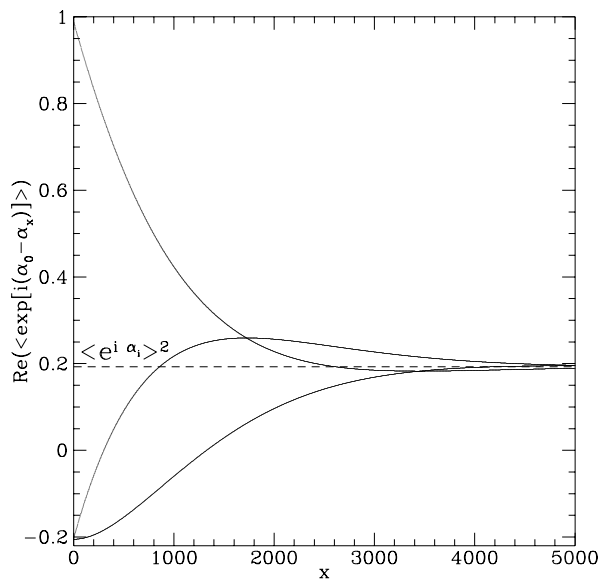


FIG. 2. Correlation function for a three periodic state ( $\Xi = 1/3$ ). The three branches correspond to  $\langle e^{i(\alpha_0 - \alpha_{3n})} \rangle$ ,  $\langle e^{i(\alpha_0 - \alpha_{3n+1})} \rangle$ , and  $\langle e^{i(\alpha_0 - \alpha_{3n+2})} \rangle$  with  $n = 0, 1, 2, \dots$ . The dotted line indicates the value of  $\langle e^{i\alpha_j} \rangle^2$ .

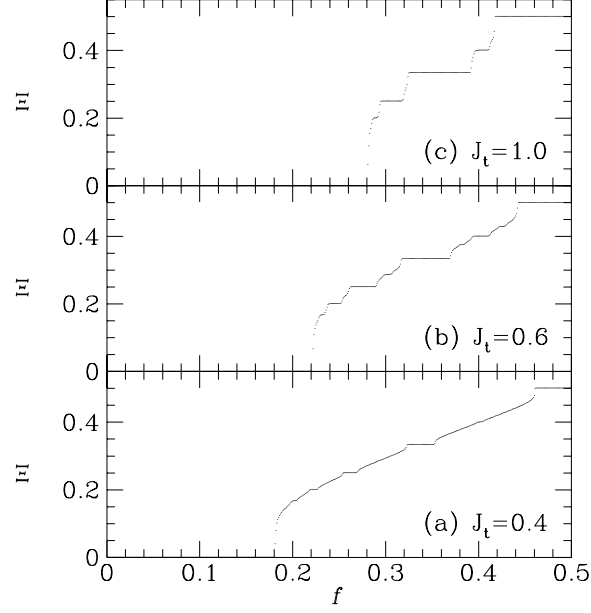


FIG. 3.  $\Xi = \text{Arg}(\lambda_1)/2\pi$  versus  $f$  for  $k_B T/J = 0.002$  and (a)  $J_t = 0.4$ , (b)  $J_t = 0.6$ , and (c)  $J_t = 1.0$ .

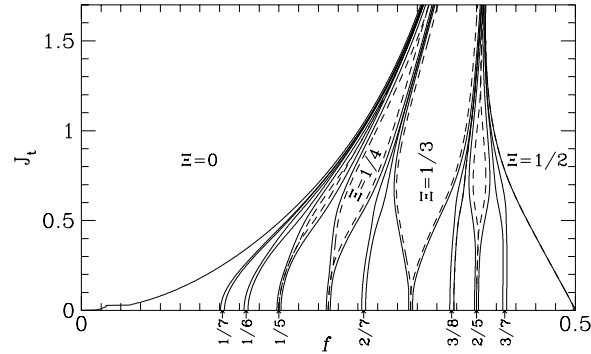


FIG. 4. Periodicity  $\Xi$  phase diagram for low order rationals. At finite temperature, the step edges are slightly rounded. The phase boundaries for a step at  $\Xi = p/q$  enclose all  $\Xi$  satisfying  $|\Xi - p/q| < \epsilon$ , with dashed lines indicating an  $\epsilon$  of  $10^{-6}$  and solid lines indicating an  $\epsilon$  of 0.002 at  $k_B T/J = 0.0007$ .

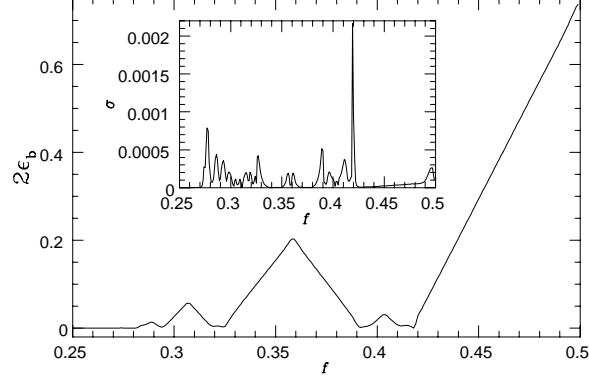


FIG. 5. Effective Ising coupling as a function of  $f$  for  $J_t = 1$ . Inset: Statistical error for  $2\epsilon_b$  in the fit versus  $f$ .

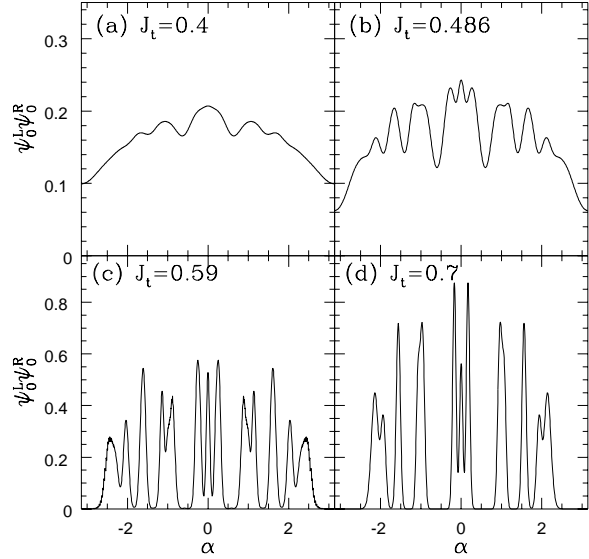


FIG. 6.  $\rho(\alpha) = \psi_0^L(\alpha)\psi_0^R(\alpha)$  versus  $\alpha$  and  $\Xi = 0.381966011\dots$ , and for (a)  $J_t = 0.4$ , (b)  $J_t = 0.486$ , (c)  $J_t = 0.59$  at  $k_B T = 0.0007J$  and (d)  $J_t = 0.7$  at  $k_B T = 0.001J$ . Note the smaller scale for the upper plots.

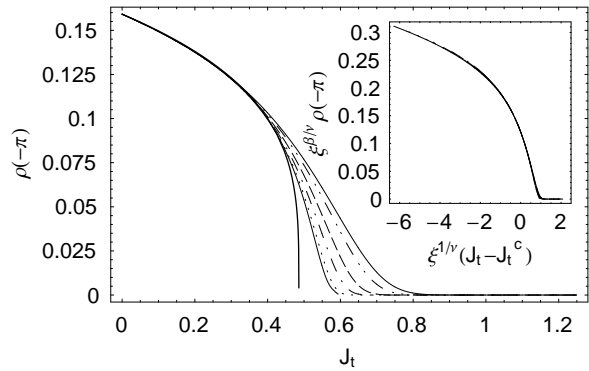


FIG. 7.  $\rho(-\pi)$  versus  $J_t$  for  $k_B T = 0.012J, 0.008J, 0.004J, 0.002J, 0.001J$ , and  $0.0007J$ . Also shown is the extrapolation to  $T = 0$ ,  $0.192257(J_t^c - J_t)^\beta$ . Inset: Scaling collapse of same data shown in main plot.

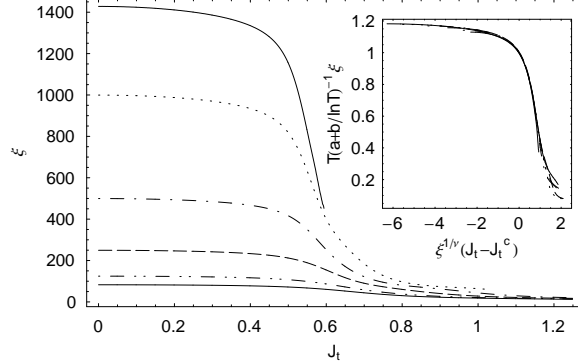


FIG. 8. Correlation length  $\xi$  versus  $J_t$  for  $k_B T = 0.012J, 0.008J, 0.004J, 0.002J, 0.001J$ , and  $0.0007J$ . Inset: Scaling collapse of same data shown in main plot ( $a = 0.793 \pm 0.006$  and  $b = -0.39 \pm 0.04$ ).

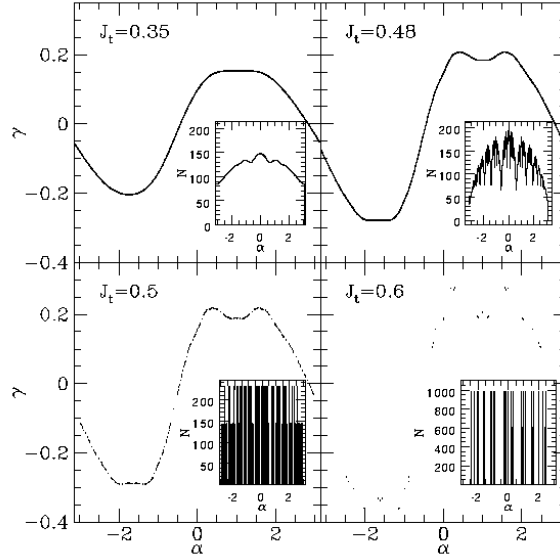


FIG. 9. KAM curves constructed from plotting each  $(\alpha_j, \gamma_j)$  as a point in the plane. The state shown is one with periodicity  $28657/75025 \approx 0.38196601$  at  $f = 28657/75025$ . Below the critical coupling  $J_t^c$ , the points fill in a smooth curve (top panels) whereas above  $J_t^c$  the points form a zero measure Cantor set. Inset: Histograms of the  $\{\alpha_j\}$ , which can be compared to the phase density  $\rho(\alpha)$  calculated from the transfer matrix

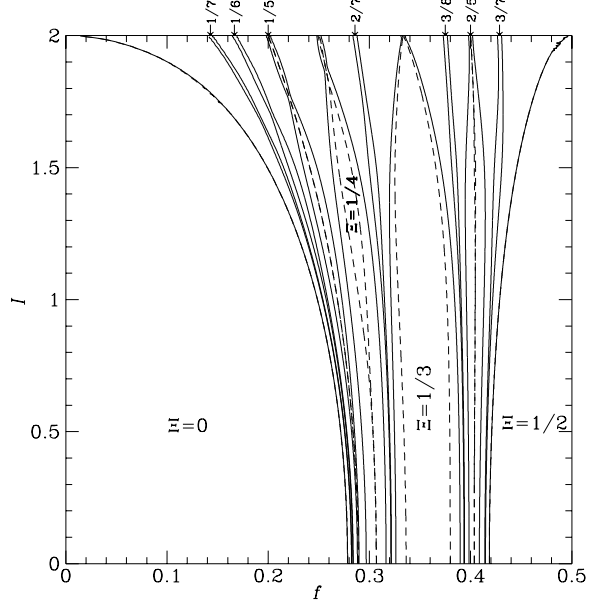


FIG. 10. Periodicity as a function of current  $I$  and filling factor  $f$  for  $J_t = 1.0$ . At finite temperature, the step edges are slightly rounded. The phase boundaries for a step at  $\Xi = p/q$  enclose all  $\Xi$  satisfying  $|\Xi - p/q| < \epsilon$ , with dashed lines indicating an  $\epsilon$  of  $10^{-6}$  and solid lines indicating an  $\epsilon$  of 0.002 at  $k_B T / J = 0.004$ . Note that some of the “tongues”, such as the one for  $\Xi = 1/4$  come to a constriction at what appears to be the critical current for that state. The section above the constriction is, therefore, above the critical current and should not be taken too seriously.